Analyst

Lensless imaging-based discrimination between tumour cells and blood cells towards circulating tumour cell cultivation

Journal:	*Analyst*
Manuscript ID	AN-ART-08-2021-001414.R1
Article Type:	Paper
Date Submitted by the Author:	09-Sep-2021
Complete List of Authors:	Maeda, Yoshiaki; Tokyo Noko Daigaku Kogakubu Daigakuin Kogaku Kenkyuin Yoshino, Tomoko; Tokyo University of Agriculture and Technology, Kogiso, Atsushi; Tokyo Noko Daigaku Kogakubu Daigakuin Kogaku Kenkyuin Negishi, Ryo; Tokyo University of Agriculture and Technology Takabayashi, Tomohiro; Tokyo Noko Daigaku Kogakubu Daigakuin Kogaku Kenkyuin Tago, Hikaru; Tokyo University of Agriculture and Technology Lim, Taekyu; Malcom Co., Ltd., Harada, Manabu; Malcom Co., Ltd., Matsunaga, Tadashi; Tokyo University of Agriculture + Technology, Department of Biotechnology Tanaka, Tsuyoshi; Tokyo University of Agriculture + Technology, Department of Biotechnology and Life Science

ARTICLE

Lensless imaging-based discrimination between tumour cells and blood cells towards circulating tumour cell cultivation

Received 00th January 20xx,
Accepted 00th January 20xx

DOI: 10.1039/x0xx00000x

Yoshiaki Maeda [a], Tomoko Yoshino [a], Atsushi Kogiso [a], Ryo Negishi [a], Tomohiro Takabayashi [a], Hikaru Tago [a], Tae-Kyu Lim [b], Manabu Harada [b], Tadashi Matsunaga [a,c], and Tsuyoshi Tanaka *[a]

Circulating tumour cells (CTCs) are recognized as important markers for cancer research. Nonetheless, the extreme rarity of CTCs in blood samples limits their availability for multiple characterizations. Cultivation of CTCs is still technically challenging due to the lack of the information of CTC proliferation, and it is difficult for conventional microscopy to monitor the CTC cultivation owing to low throughput. In addition, for precise monitoring, CTCs need to be distinguished from the blood cells which co-exist with CTCs. Lensless imaging is an emerging technique to visualize micro-objects over a wide field of view, and have been applied for various cytometric analyses including blood tests. However, discrimination between tumour cells and blood cells was not well studied. In this study, we evaluated the potential of the lensless imaging system as a tool for monitoring CTC cultivation. Cell division of model tumour cells was examined using the lensless imaging system composed of a simple setup. Subsequently, we confirmed that tumour cells, JM cells (model lymphocytes), and erythrocytes exhibited cell line-specific patterns on the lesnless images. After several discriminative parameters were extracted, discrimination between the tumour cells and other blood cells was demonstrated based on the linear discriminant analysis. We also combined the highly efficient CTC recovery device, termed microcavity array, with the lensless-imaging to demonstrate recovery, monitoring and discrimination of the tumour cells spiked into whole blood samples. This study indicates that the lensless imaging can be a powerful tool to investigate the CTC proliferation and cultivation.

Introduction

Circulating tumour cells (CTCs) are tumour cells that rarely exist in peripheral blood, and are believed to be involved in metastasis of tumours [1]. Since it was revealed that the number of CTCs in the unit volume of peripheral blood are correlated with the cancer patient prognosis and the therapeutic effects of anticancer drugs [2, 3], a variety of techniques to recover the CTCs from peripheral blood based on magnetic separation [4], filtration [5, 6], and microfluidic sorting [7, 8] have been proposed. Our group also developed various types of unique filtering devices referred to as microcavity arrays (MCAs) for highly efficient CTC recovery [9-11], and has demonstrated a wide range of CTC researches using MCAs such as automated and high-throughput recovery of CTCs [12-14], genome amplification from single CTCs [15], cell deformability assay [16], and rapid imaging of CTCs by multi-colour labelling on MCA [17].

Current trends in CTC studies more focus on the genetic analyses of the recovered CTCs with the aid of the techniques for nucleic acid amplification at a single cell level [15]. Nonetheless, unfortunately, availability of CTCs toward such characterizations is limited because of the extreme rarity of CTCs. The next challenge in this field is establishment of easy, rapid and inexpensive methods to cultivate the CTCs recovered from individual patients. It will allow us to perform various characterizations of the proliferated CTCs, and will provide useful information for personalized medicine.

Cultivation of CTCs is still technically challenging, while several successful trials have been reported [18-23]. However, the most studies failed to establish the stable cell lines derived from the recovered CTCs, although the cell proliferation in short terms (several days ~ months) were confirmed. This could be due to the lack of understandings of CTC proliferation *in vitro*. For better understanding, it is necessary to statistically analyse a large number of CTCs by contentious monitoring of the CTC proliferation at every division events. Traditionally, microscopy has been the only choice for such analyses, however, narrow field of views of microscopes limited the analysis throughput and statistical reliability.

Lensless imaging is an emerging technology for examination of biological micro-objects without conventional optical lens-systems [24, 25], and could be a powerful tool to address the issues for CTC monitoring. The lensless imaging systems consist of the 2D imaging photosensor and a light source (*e.g.*, light emitting diode (LED)). The biological micro-objects of interest are placed above the 2D photosensor, and light penetrating the objects is directly projected on the sensor (*i.e.* shadow imaging [24]). A

[a] *Division of Biotechnology and Life Science, Institute of Engineering, Tokyo University of Agriculture and Technology, 2-24-16, Naka-cho, Koganei, Tokyo, 184-8588, Japan*
[b] *Malcom Co., Ltd., 4-15-10, Honmachi, Shibuya-ku, Tokyo, 151-0071, Japan*
[c] *Japan Agency for Marine-Earth Science and Technology (JAMSTEC), 2-15, Natsushima-cho, Yokosuka, Kanagawa, 237-0061, Japan*
† Footnotes relating to the title and/or authors should appear here.
Electronic Supplementary Information (ESI) available: [details of any supplementary information available should be included here]. See DOI: 10.1039/x0xx00000x

striking feature of this system is a much wider imaging field (more than mm^2-scale) as compared to conventional microscopy which requires mechanical scanning across the mm^2-scale examination area, followed by image combining [26, 27]. The advantage of wide field of view without scanning equipments could make lensless imaging useful for various cell analyses such as CTC monitoring, which demand high throughput and/or real time monitoring.

Besides the throughput issue, another technical challenge exists in CTC monitoring; CTCs need to be distinguished from blood cells co-existing in the blood samples. Because CTCs are recovered from peripheral blood of cancer patients, the as-prepared CTC samples can contain abundant blood cells [1, 8, 10, 28], which potentially hamper the precise analysis of CTC proliferation. Therefore, lensless imaging-based discrimination between tumour cells and blood cells is an essential technique toward CTC monitoring. When cell samples were subjected to the lensless imaging, the light passing through the cells generates the images with unique patterns caused by the effects of light diffraction, scattering and interference. The unique patterns can be used for discrimination of the cell lines of interest [24]. Su et at initially proved this concept by distinguishing erythrocytes, yeast cells and polystyrene micro-beads mixed in the heterogeneous solution [29]. Seo et al in the same group further improved this system by inserting a pinhole between the light source and objects to generate coherent light [30]. Roy et al [31] and Vercruysse et al [32] applied this concept to blood test, and successfully demonstrated the discrimination of different types of leukocytes (e.g., lymphocytes, monocytes, and granulocytes). Our group also demonstrated the discrimination of microorganisms including bacteria and fungi based on the machine learning of the quantitative features extracted from lensless images of colonies in micrometer-scale (termed "colony fingerprints") [27, 33-35]. However, to the best of our knowledge, there is no study which investigates the discrimination between tumour cells and blood cells in heterogeneous mixture towards CTC cultivation.

In this study, we evaluated the potential of lensless imaging as a tool for CTC monitoring. First, time-lapse monitoring of model tumour cells (HeLa cells) were performed. Cell division event of the tumour cells was analysed by our custom-made lensless imaging system. Subsequently, lensless imaging-based discrimination between the tumour cells and blood cells were attempted. Several quantitative features were extracted from the images of the tumour cells and blood cells, and were used as discriminative parameters for multivariate analysis. At last, we performed the contentious experiments for recovery, monitoring, and discrimination of tumour cells spiked into the whole blood samples with the combined use of MCA and lensless imaging, and discussed the potential of lensless imaging towards the analysis of CTC proliferation and its contribution to CTC cultivation.

Experimental methods

Preparation of cell samples

HeLa cells and JM cells were used as model tumour cells and model lymphocytes, respectively. HeLa cells were cultured in Dulbecco's modified eagle medium (DMEM) containing 4 mM L-glutamine (Thermo Fisher SCIENTIFIC Inc., Waltham MA, USA), 10% (v/v) fetal bovine serum (FBS, Invitrogen-Thermo Fisher Scientific, Carlsbad, CA, USA), and 1% (v/v) penicillin/streptomycin (Invitrogen-Thermo Fisher Scientific, Carlsbad, CA, USA) for 3–4 days at 37 °C with 5% CO_2 supplementation. JM cells were cultured in Roswell Park Memorial Institute (RPMI) 1640 medium containing 2 mM L-glutamine (Sigma-Aldrich Co. LLC., St. Louis, MO, USA), 10% (v/v) FBS, and 1% (v/v) penicillin/streptomycin for 3–4 days at 37 °C with 5% CO_2 supplementation. To obtain erythrocytes, whole blood mixed with the same volume of Histopaque-1077 (Sigma-Aldrich Co. LLC., St. Louis, MO, USA) were centrifuged at 400x*g* for 30 min, and the resulting lower layer containing erythrocytes was collected.

Prior to each experiment, HeLa cells grown to confluence were trypsinized and re-suspended in phosphate-buffered saline (PBS) containing 0.5% bovine serum albumin (BSA) and 2 mM ethylenediaminetetraacetic acid (EDTA). HeLa cell concentrations were determined by a direct cell count using a hemocytometer.

Setup and observation

A CMOS sensor with 2048 × 1536 pixels (pixel size: 3.2 μm, imaging area: 6.55 × 4.92 mm^2, DFK61BUC02, The Imaging Source Europe GmbH, Bremen, Germany) was used for imaging. The cell culture dish (diameter: 3.5 cm) was mounted on the CMOS image sensor (Fig. 1). A blue light-emitting diode (LED) was located 10 cm above the sensor and illuminates the chamber. A blue LED was employed because light scattering effect determines the contrast of the images projected on the CMOS sensor [27]. Light with a shorter wavelength is expected to be scattered by micro-objects more strongly than that with longer wavelength, and it could result in higher contrast image of the cells against the background. The developed lensless imaging system composed of CMOS sensor and LED was kept at 37°C. Images were automatically captured every 15 min (exposure time: 1/10 sec) under the control of the IC Capture 2.2 software (The Imaging Source Europe GmbH, Bremen, Germany). After the cells in culture dishes were analysed by the this lensless imaging system, they were also observed with IN Cell Analyzer 2000 (GE Healthcare) to obtain microscopic images.

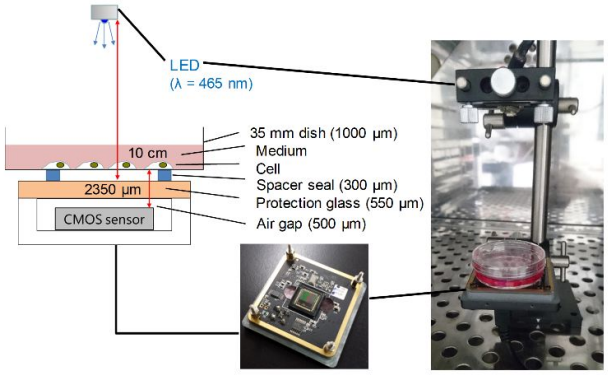

Fig. 1 A schematic diagram and photograph of the imaging system used in this study. Thickness of each component is described. The length of 2350 μm means the distance between the CMOS sensor and cells.

Extraction of discriminative parameters for multivariate analyses

The image analyses described below were performed using ImageJ [36]. The analysed cells were selected randomly from the lensless images. For discrimination of the cells, 6 discriminative parameters, minimal value, maximal value, standard deviation, and most frequently appearing value of the relative intensities (I_{min}, I_{max}, I_{sd}, and I_{mode}, respectively), difference between I_{min} and I_{max} (I_d), and cell size area (S) were extracted from the images of each cell (Table 1). Cell size area was evaluated by outlining the edge of the cells, and counting the number of the pixels in the outlined area (termed "cell region", 1 pixel = 3.2 × 3.2 μm). To calculate I_{min}, I_{max}, I_{sd}, I_{mode}, and I_d, relative intensity at a certain pixel in the cell region (I) was calculated based on the following formula, $I = I_c - I_b$, where I_c and I_b are the brightness value (ranging from 0 to 255) at a certain pixel in the cell region, and mean of the brightness value in the background region (an arbitrary area in the non-cell region with the size of 100 × 100 pixels), respectively. I_{min}, I_{max}, I_{sd} and I_{mode} were obtained by identifying or calculating the minimal, maximal, standard deviation and the most frequently appearing values of a set of I that was obtained from a cell region. Principal component analysis (PCA), *k*-means clustering, hierarchical clustering by ward's method, and linear discriminant analysis (LDA) were performed using R 3.1.2 (R Foundation for Statistical Computing, Vienna, Austria). Linear discriminant functions were generated based on three parameters, S and I_{sd} and I_d.

For the evaluation of the linear discriminant functions generated as described above, the discrimination result based on lensless imaging was compared to microscopic observation. In this experiment, HeLa cells were identified based on the GFP expression. The Hela cells which express green fluorescent protein (GFP) had been established in our previous work [37]. We confirmed that the almost all HeLa cells (~99%) showed GFP expression by fluorescence microscopy. The HeLa cells expressing GFP (approximately 1 × 10^4 cells) and JM cells (approximately 1 × 10^5 cells) were mixed in the culture dishes (3.5 cm in diameter, n = 3) containing 4 ml of the culture medium. After the cells were incubated for 18 h, the lensless images were obtained, followed by extraction of discriminative parameters from 34 lensless images of HeLa cells which were identified by GFP fluorescence afterward, and 241 lensless images of JM cells. Subsequently, the culture dishes were observed using fluorescent microscope to identify the HeLa cells according to GFP fluorescent labelling. Discrimination accuracy was determined as the percentage of the cells which were correctly estimated to be HeLa cells or JM cells based on LDA among all of the analysed cells.

Table 1 Discriminative parameters used in this study

Parameter	Abbreviation	Description [a, b]
Minimal intensity	I_{min}	The minimal value of the relative intensities in a cell region
Maximal intensity	I_{max}	The maximal value of the relative intensities in a cell region
Standard deviation of the intensities	I_{sd}	The standard deviation of the relative intensities in a cell region
Frequent intensity	I_{mode}	The value most frequently found in the relative intensities in a cell region
Intensity deference	I_d	Deference between I_{min} and I_{min}
Size of the cell area	S	Pixel number of a cell region

[a] A relative intensity at each pixel in a certain cell region was calculated by subtracting an average intensity in the square regions (100 × 100 pixels) near by the cell region from a row intensity (ranging from 0 to 255) of each pixel in the cell region.

[b] The cell regions were manually determined on the image software Image J.

Discrimination of the tumour cells recovered from blood samples using MCA device

The cell suspension containing 20, 50, and 100 cells of HeLa cells were prepared using BD FACSAria™ II (Nippon Becton Dickinson Company, Ltd., Minato-ku, Tokyo, Japan). The as-prepared HeLa cells suspensions were added in the whole blood samples (3 ml). Subsequently, the HeLa cell-spiked blood samples were treated with the microcavity array (MCA) device (8 × 100 μm² rectangular pore; the porosity of the 6 × 6 mm² array area was 6.7% [17]) and the protocol previously described [15]. The cells entrapped on the MCA were recovered by adding the 200 μl of the culture medium with pipetting action (< 1 min), encapsulated in the microchamber composed on the glass slide, cover glass and a plastic frame (7.1×5.5 mm²), and subjected to the lensless imaging (imaging area: 6.55 × 4.92 mm²). The number of the HeLa cells on the lensless images ($N_{lensless}$) was determined by LDA, and the total number of the HeLa cells recovered from the blood samples (N_{total}) were estimated using the following equation; $N_{total} = N_{lensless} \times (7.1 \times 5.5) / (6.55 \times 4.92)$.

Human blood samples were collected from healthy donors at the Tokyo University of Agriculture and Technology. Experimental protocols were approved by the Institutional Review Board of the Tokyo University of Agriculture and

Technology (Approval code: No. 30-10). Informed consents were obtained from all human subjects of this study.

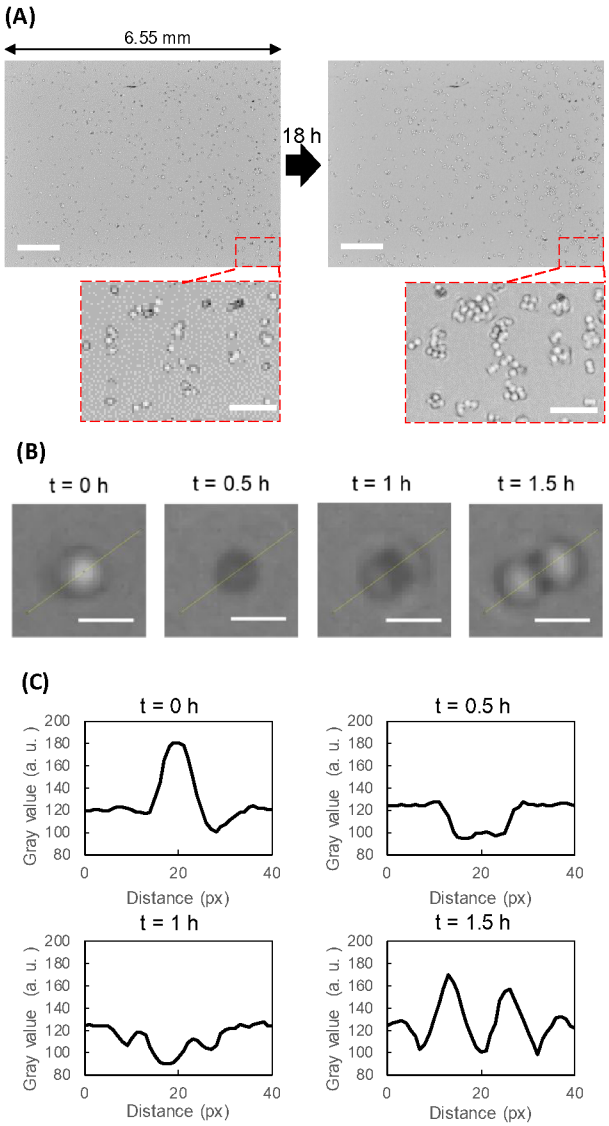

Fig. 2 Time lapse imaging of HeLa cell proliferation using the lensless imaging system. (A) Entire field-of-view images (scale bar = 1 mm) and the magnified images (scale bar = 0.25 mm) of the HeLa cell proliferating in 18 h. (B) Monitoring of the cell division event of a single HeLa cell (scale bar = 50 μm). (C) The cross sectional profiles of gray-scale values across the center of the HeLa cells during the cell division. The yellow profiling lines are shown in (B).

Results and discussion

Time-lapse monitoring of tumour cell proliferation by lensless imaging

The lensless-imaging system, we previously developed, enables time-laps monitoring of a number of cells distributed over a wide field-of-view (6.55 × 4.92 mm², corresponding to ~55 images of microscopic observation at 100× magnification) with high time resolution [27]. By taking this advantage, we demonstrated, in this study, a wide field-of-view monitoring of the proliferation of HeLa cells for 18 h (Fig. 2 (A)). At the initial time point, approximately 8×10^2 cells were visualized in the detection area (6.55 × 4.92 mm²). The cell division events were frequently observed over time (Supplementary Movie S1). Variation of the lensless images of a single HeLa cell during the cell division was shown in Figure 2 (B). Before cell division (t = 0 h), the lensless images of HeLa cells showed high intensity. Once cell division launched, the lensless images turned dark (t = 0.5 h). Subsequently, intensity recovered after the cell division (t = 1 and 1.5 h) (Fig. 2 (C)).

Next, we tested whether the cell adhesion to the bottom the culture dish affects the lensless images of HeLa cells. According to the microscopic observation, almost cells remained in the liquid culture immediately after the cells were inoculated to a flesh culture dish. After 4 h, almost cells attached on the culture dish (Supplementary Fig. S1). At such time points, HeLa cells before adhesion showed low intensity on the lensless images, whereas HeLa cells after adhesion showed relatively high intensity (Supplementary Fig. S1), indicating that cell adhesion varied the lensless images of the cells with increasing the brightness intensities.

Time-laps imaging of the cell division events of human cells by lensless imaging has been demonstrated by several groups [38-40]. As like such previous studies, our lensless imaging system could detect the changes of morphology and signal intensity of HeLa cells during the cell divisions (Fig. 2). The intensity variation of HeLa cells shown in Figure 2 (B) could be explained by the change in cell adhesion states during the cell division. Before cell division, HeLa cells showed high intensity at the central area (Fig. 2 (C), t =0 h). This is attributable to tight adhesion of HeLa cells to the bottom substrate of the culture dish (Supplementary Fig. S2). Increase in the signal intensity on lensless images caused by the cell adhesion has been also reported by Kesavan et al [39]. Following a decrease in signal intensity prior to cell division (Fig. 2 (C), t =0.5 h) could be attributable to a temporal detachment of the cells from the substrate [41]. Subsequently, two daughter cells appeared, and intensity recovered caused by re-adhesion (Fig. 2 (C), t =1.5 h). We analysed the intensity of 10 HeLa cells in the time-laps images, and confirmed the reproducibility of the intensity variations explained above (Supplementary Fig. S2). This result suggests that it is possible to predict the cell division and investigate the cell cycles using the alteration of brightness. Since it is difficult to simultaneously investigate the division evens of a number of the cells dispersed to the wide field by microscopy, this is a considerable strong point for the lensless imaging.

Discrimination between model tumour cells and blood cells

In order to discriminate tumour cells and blood cells, lensless images of HeLa cells (model tumour cells) were compared to those of JM cells (model lymphocyte) and erythrocytes. As a result, each type of the cells exhibited specific patterns on the lensless images (Fig. 3). Lensless images of the

HeLa cells have a central bright zone surrounded by a dark rim. Those of JM cells have central dark zone surrounded by a bright outermost rim. Those of erythrocytes shows lower contrast than those of HeLa cells and JM cells. We also found that the cell size on the lensless images did not exactly reflect the actual cell size on the microscopy. The sizes of typical adhesive HeLa cells, JM cell and erythrocyte were approximately 20~30, 15, and 7 μm on microscopy, respectively (Fig. 3). In contrast to the much divergent cell sizes on microscopy, the size differences of these cells on the lensless images were relatively small, whereas the cell sizes were much larger than the actual sizes detected by microscopy.

As compared to the lensless images of HeLa cells, those of JM cells and erythrocytes showed obviously low intensity (Fig. 3). This could be also, in part, attributable to the non-adhesive property of the JM cells and erythrocytes. In addition, the actual cell sizes could also affect the intensity on the lensless images. Roy and Seo et al. [42] reported that, on the lensless images, the actual micro-object size and the intensity difference between bright central region and dark edge region (termed peak-to-peak distance) shows a linear relationship, however the actual size has little correlation to the size on the lensless images. Our results are consistent with their study; HeLa cells and JM cells which were larger than erythrocytes (Fig. 3) showed higher values of I_d (intensity difference, Table 1) than that of erythrocyte (Fig. 4 (a)), while S (size of cell area, Table 1) of these three cell lines (Fig. 4 (a)) did not exactly reflect the microscopic cell size (Fig. 3). These results suggest that the actual cell size and adhesion manner strongly contributed to generation of the cell line-specific patterns on the lensless images.

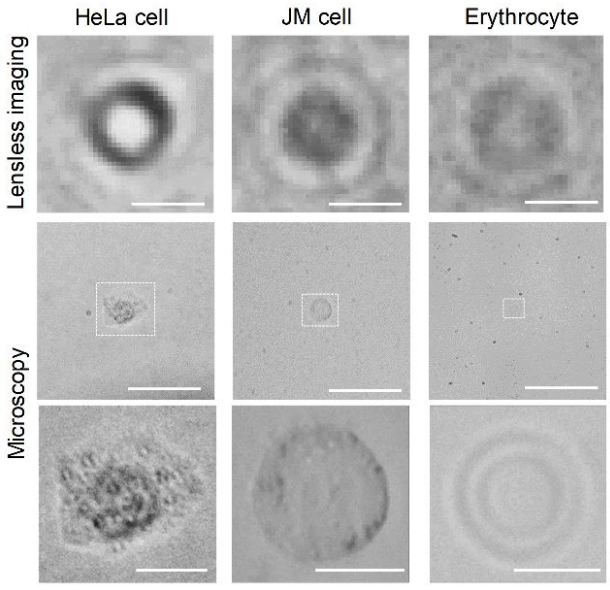

Fig 3. Typical Images of HeLa cell (model tumour cell, 8 h after seeding the cells), JM cell (model lymphocyte) and erythrocyte acquired by the lensless imaging (upper row) and microscopy (middle and lower rows). Figures in lower rows are the magnified images of the white square regions in middle row. Scale bars in upper and middle rows indicate 50 μm. Scale bars for HeLa cell, JM cell and erythrocyte in lower row indicate 15, 10, and 5 μm, respectively.

Next, we extracted 6 parameters (S, I_{min}, I_{max}, I_{sd}, I_{mode}, and I_d, Table 1) from the 40 lensless images of each cell type (120 images in total; hereinafter these data are treated as "training data"). It should be noted that the discriminative parameters were extracted from the lensless images that capture the HeLa cells and JM cells which were separately cultured, and the erythrocytes which were isolated from the whole blood. The parameters for HeLa cells were obtained from the mixtures of adhered cells and detached cells. We evaluated the distribution of the intensity of HeLa cells, and found that the presence ratio of the detached cells with low intensity was 4%. Fig. 4 (A) shows the distribution of the extracted parameters for each cell lines. The specific pattern of erythrocytes on lensless images occupied relatively larger areas than those of HeLa cells and JM cells. Lensless images of HeLa cells exhibited higher I_{max} than those of others, and it could be derived from the central bright zone. HeLa cells have higher values of I_{sd} as compared to those of others, and it could be derived from the high contrast between the central light zones and the surrounding dark zones.

In order to summarize the features of the training data, we performed principal component analysis (PCA) of the 120 data sets (40 cells of 3 cell lines; each data point contains the 6 discriminative parameters). It was found that the data sets generated from the lensless images of different cell lines were clearly separated from each other (Fig. 4 (B)). We calculated the factor loading of each parameter for PC1 and PC2, and found that I_{sd} and I_d showed strongly negative factor loadings for PC1, while I_{min} and I_{mode} showed strongly positive factor loadings (Supplementary Table S1). Since the data points of HeLa cells showed negative values in the direction of PC1, the separation of HeLa cells on PCA could be attributable to the high values of I_{sd} and I_d (in other words, high contrast) of HeLa cells (Fig. 4 (A)). On the other hand, JM cells and erythrocytes were particularly separated in the direction of PC2 as well. The cell size area on the lensless images (S) showed relatively strong contribution to the separation of three cell lines in the direction of PC2, and thus this parameter could be also important to discriminate the cell lines.

When the 120 data sets were classified by hierarchical clustering (ward's method), images of HeLa cells, JM cells and erythrocytes were clustered in three different clades, respectively, with an exception of an image of HeLa cells which were included in the clade of JM cells (Supplementary Fig. S3). We also performed non-hierarchical clustering (*k*-means clustering), which was set to generate 3 clusters. As a result, all 3 clusters were composed of 40 data sets derived from identical cell lines (Fig. 4 (B)).

In order to discriminate the HeLa cells as model tumour cells from blood cells based on the discriminative parameters, linear discriminant analysis (LDA) was performed. Here, we employed three discriminative parameters of S, I_{sd}, and I_d. These 3 parameters strongly contributed to the separation of the data sets on PCA, implying that the values of these parameters of the 3 cell lines tend to be different from each other. First, 120 data sets (40 cells for 3 cell lines, respectively) of the training data was analysed, and 2 discriminant functions (LD1 and LD2) were generated as below.

$$LD1=(-0.0091)\times S+0.3376\times I_{sd}+0.0358\times I_d$$
$$LD2=(-0.0446)\times S+0.0304\times I_{sd}+(-0.0477)\times I_d$$

The values of the discrimination functions were obviously separated between HeLa cells, JM cells, and erythrocytes (Supplementary Fig. S4), and discrimination accuracy for the training data was 100%.

Subsequently, we evaluated the linear discriminative functions by discriminating the prediction data set of the cells in the heterogeneous cell solution. In this experiment, we used the genetically engineered HeLa cells which expressed GFP, and attempted to discriminate between the GFP-expressing HeLa cells and JM cells, which were mixed in the heterogeneous cell solution (Fig. 5 (A) and (B)). The reason why these two cell lines were chosen for evaluation is because these two cell lines relatively resemble to each other according to hierarchical clustering (Fig. S3). The prediction data set consisting of the lensless images of 34 HeLa cells (GFP fluorescence was confirmed by microscopy) and 241 JM cells in the heterogeneous cell mixture. As a result, based on the LD1 and LD2 generated from 3 parameters of S, I_{sd} and I_d, only 1 HeLa cell and 2 JM cells were faultily classified into JM cells and HeLa cells, respectively (Fig. 5 (C)), indicating that the discriminant accuracy was approximately 99%.

Although LDA was able to discriminate HeLa cells and JM cells with 99% of accuracy, there were three cells which were incorrectly classified; one HeLa cells (HeLa_No.9 in Supplementary Fig. S5) was classified into JM cells, and two JM cells (JM_No.185 and JM_No.187) were classified into HeLa cells. HeLa_No.9 showed obviously low values of I_{sd} and I_d (i.e., low contrast) as compared to other HeLa cells (Supplementary Fig. S5), and this could be because this cell was during the cell division at the analysed time point as with the cells shown in Figure 2 (B). This issue can be solved by performing LDA at other time points, at which the target cells were not during the cell division. Lensless imaging allows us to perform the time-laps imaging (Fig. 2), and thus it could be easy to select the appropriate images. By contrast, JM_No.185 and JM_No.187 showed relatively higher I_{sd} and I_d (i.e., high contrast) as compared to other JM cells (Supplementary Fig. S5). Although the reason why these cells showed high contrast is not clear, these cells might have larger cell size, leading to higher contrast on the lensless images.

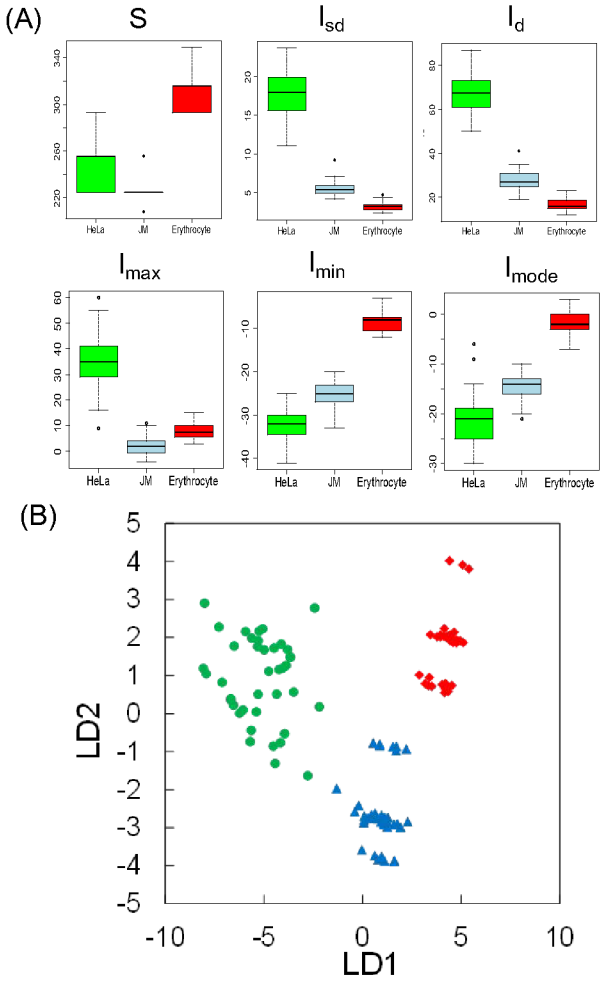

Fig 4. Discriminative parameters (Area, I_{sd}, I_d, I_{max}, I_{min} and I_{mode}) extracted from the lensless images of 40 cells of HeLa cells (green marks, model tumour cells), JM cells (blue marks, model lymphocytes) and erythrocytes (red marks). (A) Boxplots of each parameter. (B) Linear discriminant analysis (LDA) of 3 (S, I_{sd}, and I_d) parameters. Scattered plots represent the distribution of the values of liner discriminant functions derived from 40 cells of HeLa cells (green), JM cells (blue) and erythrocytes (red), which were separately cultured in different culture dishes.

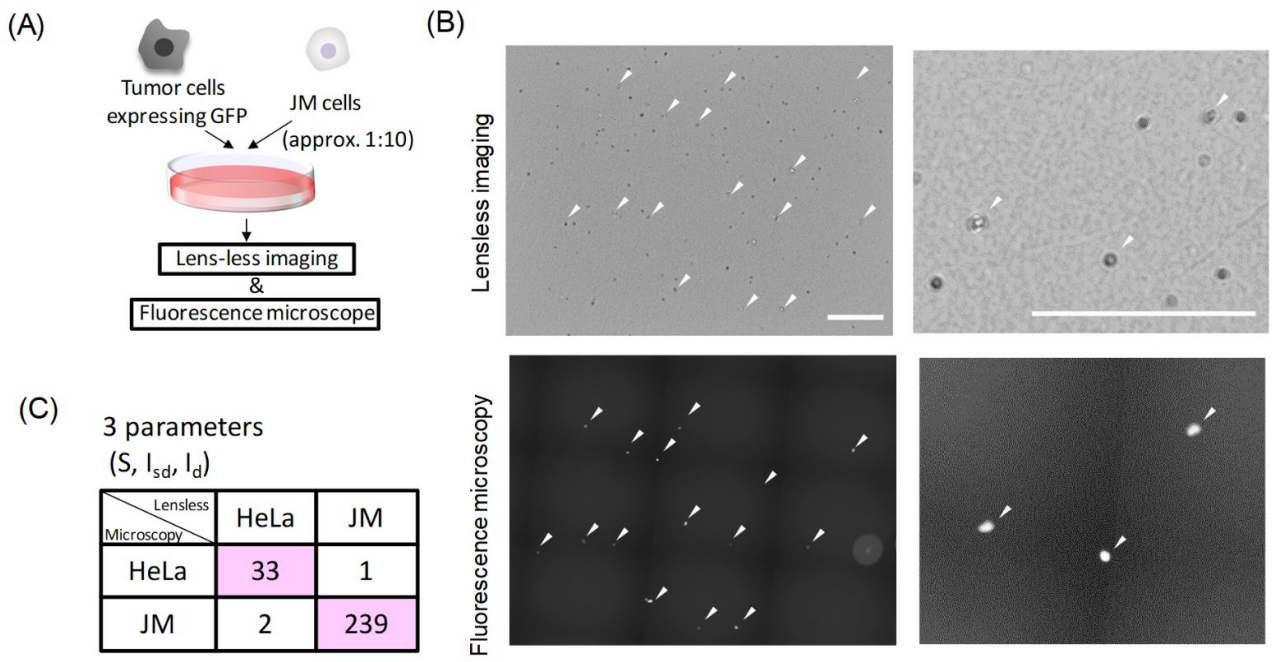

Lensless / Microscopy	HeLa	JM
HeLa	33	1
JM	2	239

Fig 5. Linear discriminant analysis (LDA) of the lensless images of HeLa cells (model tumour cells) and JM cells (model lymphocytes). (A) Schematic drawing of the discrimination experiment using GFP-expressing HeLa cells and JM cells. (B) Lensless and fluorescence microscopic images of the heterogeneous cell solution of the GFP-expressing HeLa cells (white triangles) and JM cells (scale bar = 1 mm). (C) Discrimination result based on the LDA of three discriminative parameters (S, I_{sd}, and I_d). The numbers in pink color is the cells correctly classified.

Discrimination of the tumour cells recovered from blood samples using MCA device

For the demonstration of the tumour cell discrimination from whole blood samples, certain number (20, 50, and 100 cells) of HeLa cells were spiked in the whole blood samples, recovered from the blood sample using MCA device, and analysed by lensless imaging. The number of the HeLa cells on the lensless images were determined using LD1 and LD2 described above, and the total number of the HeLa cells recovered from the blood samples were estimated (see Materials and Methods). When 100, 50, and 20 HeLa cells were spiked in the blood samples (n = 3, respectively), it was estimated that 76 ± 5 (70, 76, 80), 34 ± 1 (35, 35, 33), and 18 ± 3 (18, 21, 15) cells were recovered from the blood samples.

The model discrimination experiments in which the HeLa cells spiked in the whole blood were recovered by MCA, followed by monitoring and discrimination by lensless imaging, proved the potential of the lensless imaging system developed in this study for CTC research. It was reasonable that the number of the cells recognized as HeLa cells based on lensless imaging increased with increasing the number of the cell initially spiked in the blood sample. Nonetheless, the number of the HeLa cells detected by lensless imaging was 77.7±12.0% of the number of the HeLa cells initially spiked in the blood samples. Given the high recovery efficiency of MCA (typically >97 % [11]) and high discrimination accuracy of lensless imaging, loss of the HeLa cells might occur when they were recovered from MCA by pipetting action. The protocol for tumour cell recovery from MCA is still under the optimization, and should be improved in the future study.

The adhesive property of tumour cells is one of the important factor for accurate discrimination based on the lensless imaging. Adhesion and extension of the cells to the bottom surface of culture dishes is the essential events for CTC to proliferate in the following cultivation [43, 44]. Therefore, it is reasonable to discriminate the cancer cells and blood cells based on the parameters which were strongly affected by the cell adhesion behaviours. On the other hand, an opposite example was also reported; non-adherent culture conditions were critical for successful cultivation [18]. How the adhesive property of the CTCs affects the cultivation performance is still a matter of debate, and thus further investigations need to be performed for characterization of adhesive and non-adhesive CTCs. In addition, the discrimination required incubation time, at least 4 h in this study, to filopodia extension. Because rapid discrimination is another important factor for this system, but was not fully investigated in the present proof-of-concept. We will study this point in the future study.

Lensless imaging has a number of advantageous features such as simple, compact and inexpensive setups, and significantly wide field of view capable of capturing hundreds to thousands of cells in one shot. Therefore, lensless imaging will show considerable promise in high throughput screening of CTC culture conditions. For instance, Ghogel et al reported the development of a high throughput screening system based on lensless imaging [45]. They combined a 12×8 CMOS image sensors array and a transparent-bottomed 96-well, and performed the wound healing assay. Lensless-imaging based high throughput screening systems will be applicable for monitoring a large

number of CTCs which are cultured under different culture conditions.

Conclusions

We developed a lensless imaging system for monitoring tumour cell proliferation toward CTC cultivation. Using the developed system, time-laps imaging of cell division events of the model tumour cells (HeLa cells) could be performed over a wide field of view (6.55 × 4.92 mm^2). We found that HeLa cells, JM cells (model lymphocyte), and erythrocytes exhibited cell line-specific patterns on the lensless images. Discriminative parameters were extracted from the lesnless images of the three different cell lines. LDA based on the extracted parameters successfully discriminated HeLa cells and other cell lines with high accuracy. Furthermore, it was also suggested that the lensless imaging-based discrimination was applicable to the HeLa cells recovered from the whole blood samples using the MCA devices. These results suggest that the lensless imaging is a promising technique to monitor the CTCs, and can be a powerful tool to obtain useful information regarding CTC cultivation in the future study.

Author Contributions

Yoshiaki Maeda: Formal analysis, Data curation, Visualization, Writing – original draft; Tomoko Yoshino: Conceptualization, Writing – review & editing; Atsushi Kogiso: Investigation; Ryo Negishi: Methodology, Investigation; Tomohiro Takabayashi: Investigation; Hikaru Tago: Formal analysis, Visualization, Writing – review & editing; Tae-Kyu Lim: Formal analysis, Writing – review & editing; Manabu Harada: Formal analysis, Writing – review & editing; Tadashi Matsunaga: Formal analysis, Writing – review & editing; Tsuyoshi Tanaka: Conceptualization, Formal analysis, Writing – review & editing

Conflicts of interest

There are no conflicts to declare.

Acknowledgements

This study is, in part, supported by Program on Open Innovation Platform with Enterprises, Research Institute and Academia (OPERA).

References

1. M. Cristofanilli, G. T. Budd, M. J. Ellis, A. Stopeck, J. Matera, M. C. Miller, J. M. Reuben, G. V. Doyle, W. J. Allard, L. W. Terstappen and D. F. Hayes, *The New England journal of medicine*, 2004, **351**, 781-791.
2. S. Nakamura, H. Yagata, S. Ohno, H. Yamaguchi, H. Iwata, N. Tsunoda, Y. Ito, N. Tokudome, M. Toi, K. Kuroi and E. Suzuki, *Breast cancer (Tokyo, Japan)*, 2010, **17**, 199-204.
3. S. Tarumi, M. Gotoh, Y. Kasai, N. Matsuura, M. Okuda, T. Go, S. Ishikawa and H. Yokomise, *Journal of cardiothoracic surgery*, 2013, **8**, 175.
4. S. J. Cohen, C. J. Punt, N. Iannotti, B. H. Saidman, K. D. Sabbath, N. Y. Gabrail, J. Picus, M. Morse, E. Mitchell, M. C. Miller, G. V. Doyle, H. Tissing, L. W. Terstappen and N. J. Meropol, *Journal of clinical oncology : official journal of the American Society of Clinical Oncology*, 2008, **26**, 3213-3221.
5. S. Zheng, H. Lin, J. Q. Liu, M. Balic, R. Datar, R. J. Cote and Y. C. Tai, *Journal of chromatography. A*, 2007, **1162**, 154-161.
6. T. Suzuki, N. Kaji, H. Yasaki, T. Yasui and Y. Baba, *Analytical chemistry*, 2020, **92**, 2483-2491.
7. S. Nagrath, L. V. Sequist, S. Maheswaran, D. W. Bell, D. Irimia, L. Ulkus, M. R. Smith, E. L. Kwak, S. Digumarthy, A. Muzikansky, P. Ryan, U. J. Balis, R. G. Tompkins, D. A. Haber and M. Toner, *Nature*, 2007, **450**, 1235-1239.
8. E. Ozkumur, A. M. Shah, J. C. Ciciliano, B. L. Emmink, D. T. Miyamoto, E. Brachtel, M. Yu, P. I. Chen, B. Morgan, J. Trautwein, A. Kimura, S. Sengupta, S. L. Stott, N. M. Karabacak, T. A. Barber, J. R. Walsh, K. Smith, P. S. Spuhler, J. P. Sullivan, R. J. Lee, D. T. Ting, X. Luo, A. T. Shaw, A. Bardia, L. V. Sequist, D. N. Louis, S. Maheswaran, R. Kapur, D. A. Haber and M. Toner, *Science translational medicine*, 2013, **5**, 179ra147.
9. M. Hosokawa, T. Hayata, Y. Fukuda, A. Arakaki, T. Yoshino, T. Tanaka and T. Matsunaga, *Analytical chemistry*, 2010, **82**, 6629-6635.
10. M. Hosokawa, T. Yoshikawa, R. Negishi, T. Yoshino, Y. Koh, H. Kenmotsu, T. Naito, T. Takahashi, N. Yamamoto, Y. Kikuhara, H. Kanbara, T. Tanaka, K. Yamaguchi and T. Matsunaga, *Analytical chemistry*, 2013, **85**, 5692-5698.
11. M. Hosokawa, H. Kenmotsu, Y. Koh, T. Yoshino, T. Yoshikawa, T. Naito, T. Takahashi, H. Murakami, Y. Nakamura, A. Tsuya, T. Shukuya, A. Ono, H. Akamatsu, R. Watanabe, S. Ono, K. Mori, H. Kanbara, K. Yamaguchi, T. Tanaka, T. Matsunaga and N. Yamamoto, *PloS one*, 2013, **8**, e67466.
12. R. Negishi, M. Hosokawa, S. Nakamura, H. Kanbara, M. Kanetomo, Y. Kikuhara, T. Tanaka, T. Matsunaga and T. Yoshino, *Biosensors & bioelectronics*, 2015, **67**, 438-442.
13. R. Negishi, H. Saito, R. Iwata, T. Tanaka and T. Yoshino, *Engineering in life sciences*, 2020, **20**, 485-493.
14. R. Negishi, K. Takai, T. Tanaka, T. Matsunaga and T. Yoshino, *Analytical chemistry*, 2018, **90**, 9734-9741.
15. T. Yoshino, T. Tanaka, S. Nakamura, R. Negishi, M. Hosokawa and T. Matsunaga, *Analytical chemistry*, 2016, **88**, 7230-7237.
16. T. Yoshino, T. Tanaka, S. Nakamura, R. Negishi, N. Shionoiri, M. Hosokawa and T. Matsunaga, *Analytical biochemistry*, 2017, **520**, 16-21.
17. T. Yoshino, K. Takai, R. Negishi, T. Saeki, H. Kanbara, Y. Kikuhara, T. Matsunaga and T. Tanaka, *Analytica chimica acta*, 2017, **969**, 1-7.
18. M. Yu, A. Bardia, N. Aceto, F. Bersani, M. W. Madden, M. C. Donaldson, R. Desai, H. Zhu, V. Comaills, Z. Zheng, B. S. Wittner, P. Stojanov, E. Brachtel, D. Sgroi, R. Kapur, T. Shioda, D. T. Ting, S. Ramaswamy, G. Getz, A. J. Iafrate, C. Benes, M. Toner, S. Maheswaran and D. A. Haber, *Science (New York, N.Y.)*, 2014, **345**, 216-220.

19. Z. Zhang, H. Shiratsuchi, J. Lin, G. Chen, R. M. Reddy, E. Azizi, S. Fouladdel, A. C. Chang, L. Lin, H. Jiang, M. Waghray, G. Luker, D. M. Simeone, M. S. Wicha, D. G. Beer, N. Ramnath and S. Nagrath, *Oncotarget*, 2014, **5**, 12383-12397.
20. L. Cayrefourcq, T. Mazard, S. Joosse, J. Solassol, J. Ramos, E. Assenat, U. Schumacher, V. Costes, T. Maudelonde, K. Pantel and C. Alix-Panabieres, *Cancer research*, 2015, **75**, 892-901.
21. D. Brungs, E. Minaei, A. K. Piper, J. Perry, A. Splitt, M. Carolan, S. Ryan, X. J. Wu, S. Corde, M. Tehei, M. Aghmesheh, K. L. Vine, T. M. Becker and M. Ranson, *Scientific reports*, 2020, **10**, 539.
22. Z. Que, B. Luo, Z. Zhou, C. Dong, Y. Jiang, L. Wang, Q. Shi and J. Tian, *Cancer cell international*, 2019, **19**, 21.
23. J. Kapeleris, A. Kulasinghe, M. E. Warkiani, C. Oleary, I. Vela, P. Leo, P. Sternes, K. O'Byrne and C. Punyadeera, *Translational lung cancer research*, 2020, **9**, 1795-1809.
24. A. Ozcan and E. McLeod, *Annual review of biomedical engineering*, 2016, **18**, 77-102.
25. T. Tanaka, T. Yoshino, Y. Maeda, T. Saeki, R. Negishi, R. Iwata, A. Kogiso, H. Dobashi and T. Matsunaga, *ECS Transactions*, 2016, **75**, 139-146.
26. T. Tanaka, T. Saeki, Y. Sunaga and T. Matsunaga, *Biosensors & bioelectronics*, 2010, **26**, 1460-1465.
27. Y. Maeda, H. Dobashi, Y. Sugiyama, T. Saeki, T. K. Lim, M. Harada, T. Matsunaga, T. Yoshino and T. Tanaka, *PloS one*, 2017, **12**, e0174723.
28. M. S. Kim, T. S. Sim, Y. J. Kim, S. S. Kim, H. Jeong, J. M. Park, H. S. Moon, S. I. Kim, O. Gurel, S. S. Lee, J. G. Lee and J. C. Park, *Lab on a chip*, 2012, **12**, 2874-2880.
29. T. W. Su, S. Seo, A. Erlinger and A. Ozcan, *Biotechnology and bioengineering*, 2009, **102**, 856-868.
30. S. Seo, T. W. Su, D. K. Tseng, A. Erlinger and A. Ozcan, *Lab on a chip*, 2009, **9**, 777-787.
31. M. Roy, G. Jin, D. Seo, M.-H. Nam and S. Seo, *Sensors and Actuators B: Chemical*, 2014, **201**, 321-328.
32. D. Vercruysse, A. Dusa, R. Stahl, G. Vanmeerbeeck, K. de Wijs, C. Liu, D. Prodanov, P. Peumans and L. Lagae, *Lab on a chip*, 2015, **15**, 1123-1132.
33. Y. Maeda, Y. Sugiyama, A. Kogiso, T. K. Lim, M. Harada, T. Yoshino, T. Matsunaga and T. Tanaka, *Sensors* 2018, **18**.
34. Y. Maeda, Y. Sugiyama, T. K. Lim, M. Harada, T. Yoshino, T. Matsunaga and T. Tanaka, *Biosensors & bioelectronics*, 2019, **146**, 111747.
35. T. Tanaka, A. Kogiso, Y. Maeda and T. Matsunaga, 2019.
36. C. A. Schneider, W. S. Rasband and K. W. Eliceiri, *Nat Methods*, 2012, **9**, 671-675.
37. T. Mori, M. Murata, T. Yoshino, S. Nakasono, F. Saito, H. Takeyama and T. Matsunaga, *Toxicology letters*, 2009, **186**, 123-129.
38. G. Jin, I. H. Yoo, S. P. Pack, J. W. Yang, U. H. Ha, S. H. Paek and S. Seo, *Biosensors & bioelectronics*, 2012, **38**, 126-131.
39. S. V. Kesavan, F. Momey, O. Cioni, B. David-Watine, N. Dubrulle, S. Shorte, E. Sulpice, D. Freida, B. Chalmond, J. M. Dinten, X. Gidrol and C. Allier, *Scientific reports*, 2014, **4**, 5942.
40. G. Zheng, S. A. Lee, Y. Antebi, M. B. Elowitz and C. Yang, *Proceedings of the National Academy of Sciences of the United States of America*, 2011, **108**, 16889-16894.
41. M. Thery and M. Bornens, *Current opinion in cell biology*, 2006, **18**, 648-657.
42. M. Roy, D. Seo, C. H. Oh, M. H. Nam, Y. J. Kim and S. Seo, *Biosensors & bioelectronics*, 2015, **67**, 715-723.
43. M. Vishnoi, S. Peddibhotla, W. Yin, T. S. A, G. C. George, D. S. Hong and D. Marchetti, *Scientific reports*, 2015, **5**, 17533.
44. J. Y. Chen, W. S. Tsai, H. J. Shao, J. C. Wu, J. M. Lai, S. H. Lu, T. F. Hung, C. T. Yang, L. C. Wu, J. S. Chen, W. H. Lee and Y. C. Chang, *PloS one*, 2016, **11**, e0149633.
45. I. Ghorbel, F. Kermarrec, B. Sartor, X. Gidrol and V. Haguet, presented in part at the 18th International Conference on Miniaturized Systems for Chemistry and Life Sciences, MicroTAS 2014, San Antonio, Texas, USA, 2014.